**The isoforms of pyruvate kinase act as nutrient sensors for the β-cell $K_{ATP}$ channel**

Hannah R. Foster[1], Thuong Ho[1], Evgeniy Potapenko[1], Sophia M. Sdao[1], Sophie L. Lewandowski[1], Halena R. VanDeusen[1], Shawn M. Davidson[2,3], Rebecca L. Cardone[4], Richard G. Kibbey[4,5], and Matthew J. Merrins[1,6*]

[1]Department of Medicine, Division of Endocrinology, Diabetes, and Metabolism, University of Wisconsin-Madison, Madison, WI, USA
[2]Koch Institute for Integrative Cancer Research, Massachusetts Institute of Technology, Cambridge, MA, USA
[3]Lewis-Sigler Institute for Integrative Genomics, Princeton University, Princeton, NJ, USA
[4]Department of Internal Medicine, Yale University, New Haven, CT, USA
[5]Department of Cellular & Molecular Physiology, Yale University, New Haven, CT, USA
[6]William S. Middleton Memorial Veterans Hospital, Madison, WI, USA
*Correspondence: mmerrins@medicine.wisc.edu

The authors have declared that no conflict of interest exists.

## SUMMARY

Insulin release from pancreatic β-cells is triggered by the metabolism-dependent closure of ATP-sensitive $K^+$ ($K_{ATP}$) channels. Here, we used isoform-specific deletion of pyruvate kinase (PK) to identify the unique roles of PKm1 and PKm2 in the β-cell nutrient response. In the absence of PK activity, cytosolic ATP/ADP was insufficient to close $K_{ATP}$ channels. Both PK isoforms were found on the plasma membrane, where they endow $K_{ATP}$ channels with nutrient sensitivity and specificity. Although PKm1 accounts for >90% of cellular activity, PKm2 controls glucose-dependent $K_{ATP}$ closure. Amino acids, which generate mitochondrial phosphoenolpyruvate (PEP) without allosterically activating PKm2, depend on PKm1 to raise ATP/ADP and close $K_{ATP}$ channels. Shifting the β-cell from PKm2 to PKm1 correspondingly increased amino acid sensitivity and boosted secretory output. In addition to these membrane depolarizing "on-switches," β-cell deletion of PCK2 exposed a mitochondrial PEP-dependent "off-switch" that facilitates $Ca^{2+}$ extrusion. Restricting PCK2 prolonged $Ca^{2+}$ influx and increased insulin secretion. In summary, it is not the $K_{ATP}$ channel alone, but the PK-$K_{ATP}$ microcompartment that confers nutrient sensitivity to the β-cell plasma membrane. The differential response of the PK isoforms to the glycolytic and mitochondrial sources of PEP influences β-cell nutrient preference, and controls the oscillatory cycle regulating insulin secretion.

## KEYWORDS

Pyruvate kinase, phosphoenolpyruvate, PKm1, PKm2, PCK2, $K_{ATP}$ channels, β-cell metabolism, PEP cycle, ATP/ADP, $Ca^{2+}$ oscillations, insulin secretion

## INTRODUCTION

Maintenance of euglycemia relies on β-cells to couple nutrient sensing with appropriate insulin secretion. Insulin release is stimulated by the metabolism-dependent closure of ATP-sensitive $K^+$ ($K_{ATP}$) channels (Ashcroft et al., 1984; Cook and Hales, 1984; Rorsman and Trube, 1985), which triggers $Ca^{2+}$ influx and exocytosis (Anderson and Long, 1947; Grodsky et al., 1963). Contrary to what is often believed, the glucose-induced signaling process in β-cells has not been largely solved, and the entrenched model (Campbell and Newgard, 2021; Prentki et al., 2013; Thompson and Satin, 2021) implicating a rise in mitochondrially-derived ATP driving $K_{ATP}$ channel closure is likely wrong, the main reason being that it does not account for the thermodynamic principle of mitochondrial respiratory control (Corkey, 2020; Lewandowski et al., 2020; Nicholls, 2016). The recent discovery that pyruvate kinase (PK), which converts ADP and phosphoenolpyruvate (PEP) to ATP and pyruvate, is present on the plasma membrane and sufficient to close $K_{ATP}$ channels (Lewandowski et al., 2020), provides a potential resolution to this decades-old problem. As such, Lewandowski *et al.* proposed a revised model of β-cell fuel sensing, which we refer to here as the $Mito_{Cat}$-$Mito_{Ox}$ model, that is relevant to human islets and the in vivo context (Abulizi et al., 2020; Lewandowski et al., 2020).

In this oscillatory model of β-cell metabolism, $Ca^{2+}$ and ADP availability dictate the metabolic cycles that preferentially occur during the electrically-silent triggering phase or the electrically-active secretory phase of glucose-stimulated oscillations (Figure S1). During the triggering phase, the favorable bioenergetics of PK-driven PEP metabolism progressively lowers ADP and slows oxidative phosphorylation, precluding mitochondria from generating ATP/ADP near $K_{ATP}$ in a phase of metabolism termed $Mito_{Cat}$ (a.k.a. $Mito_{Synth}$ (Lewandowski et al., 2020)). The shift to a higher $\Delta\Psi_m$ and ATP/ADP ratio elevates the NADH/$NAD^+$ ratio in the mitochondrial matrix and stalls the TCA cycle. The ensuing increase in acetyl-CoA allosterically activates pyruvate carboxylase, the anaplerotic consumer of pyruvate that fuels oxaloacetate-dependent PEP cataplerosis by mitochondrial PEP carboxykinase (PCK2). The return of mitochondrial PEP to the cytosol completes the "PEP cycle" that augments ATP/ADP generation by cytosolic PK, which is sufficient to close $K_{ATP}$ channels. Following membrane depolarization, the increased workload (ATP hydrolysis) associated with $Ca^{2+}$ extrusion and exocytosis elevates ADP, which activates oxidative phosphorylation to sustain the secretory phase in a phase referred to as $Mito_{Ox}$. As genetic evidence for the $Mito_{Cat}$-$Mito_{Ox}$ model is presently lacking, an unresolved aspect is whether a mitochondrially-dependent rise in bulk cytosolic ATP/ADP is sufficient to close $K_{ATP}$ channels, or whether compartmentalized PK activity is strictly required.

In the $Mito_{Cat}$-$Mito_{Ox}$ model, PK has two possible sources of PEP that may differentially regulate $K_{ATP}$ closure: glycolytic PEP produced by enolase, and mitochondrial PEP produced by PCK2 in response to anaplerosis (Figure 1a). About 40% of glucose-derived PEP is generated by PCK2 in the PEP cycle and closely linked to insulin secretion (Abulizi et al., 2020; Jesinkey et al., 2019; Stark et al., 2009), suggesting a role in glucose-stimulated oscillations. Mitochondrial PEP derived from PCK2 may provide a glycolysis-independent mechanism by which PK rapidly

increases the cytosolic ATP/ADP ratio locally at the $K_{ATP}$ channel in response to amino acids, which are potent anaplerotic fuels.

The isoforms of PK, each with different activities and mechanisms of control, may also be important regulators of $K_{ATP}$ channel closure (Figure 1a). β-cells express the constitutively-active PKm1 as well as two allosterically-recruitable isoforms, PKm2 and PKL, which are activated by glycolytic fructose-1,6-bisphosphate (FBP) generated upstream by the phosphofructokinase-1 reaction (DiGruccio et al., 2016; MacDonald and Chang, 1985; Mitok et al., 2018). Pharmacologic PK activators (PKa), which lower the $K_m$ of PKm2 for PEP and increase $V_{max}$ (Anastasiou et al., 2012), increase the frequency of glucose-stimulated $Ca^{2+}$ and ATP/ADP oscillations and potentiate nutrient-stimulated insulin secretion from rodent and human islets (Abulizi et al., 2020; Lewandowski et al., 2020). Much less is known about the PKm1 isoform, whose constitutive activity may be ideal in situations of high oxidative workload, as in cardiac myocytes (Li et al., 2021, p. 1). β-cells may shift their reliance upon different PK isoforms throughout the oscillatory cycle, as the levels of glycolytic FBP rise during $Mito_{Cat}$ and fall during $Mito_{Ox}$ (Lewandowski et al., 2020; Merrins et al., 2016, 2013).

Here, we show for the first time that PK is essential for $K_{ATP}$ closure – mitochondrial fuels can effectively raise cytosolic ATP/ADP but cannot close $K_{ATP}$ channels without PK. We further demonstrate that both PKm1 and PKm2 are active in the $K_{ATP}$ channel microcompartment with at least two required functions. First, shared control over $K_{ATP}$ closure provides redundancy in the β-cell response to glucose. Such spatial privilege permits the minor PKm2 isoform, when activated by FBP, to transmit the signal from glucose to $K_{ATP}$ despite contributing a small fraction of the whole cell PK activity. Second, the composition of PK isoforms within the compartment tunes the β-cell response to amino acids, which provide mitochondrial PEP without also generating the FBP needed to allosterically activate PKm2. β-cell PCK2, in the mitochondria, signals to the plasma membrane $K_{ATP}$ microcompartment during $Mito_{Cat}$ and is essential for cytosolic ATP/ADP generation. In addition, PCK2 signals via PKm2 to facilitate $Ca^{2+}$ extrusion during $Mito_{Ox}$. These data refine the $Mito_{Cat}$-$Mito_{Ox}$ model of oscillatory metabolism by identifying unique functions of the PKm1- and PKm2-driven PEP cycles in β-cell nutrient sensing.

## RESULTS

*PKm1 accounts for >90% of β-cell PK activity with only a small contribution from PKm2*

We generated β-cell specific PKm1 and PKm2 knockout mice by breeding *Ins1-Cre* mice (Thorens et al., 2015) with *Pkm1*$^{f/f}$ mice (Davidson et al., 2021; Li et al., 2021) (PKm1-βKO) or *Pkm2*$^{f/f}$ mice (Israelsen et al., 2013) (PKm2-βKO). PKm1 protein was reduced by 71% in PKm1-βKO islets, while PKm2 increased by 46% compared to littermate *Ins1-Cre* controls (Figure 1b). Comparatively, expression of PKm2 protein fell by 94% in PKm2-βKO islets, while PKm1 increased by 29% (Figure 1c). In both strains this partial compensation is expected since PKm1 and PKm2 are alternative splice variants of the *Pkm* gene (Li et al., 2021; Israelsen et al., 2013). *Pck2*$^{f/f}$ mice were generated *de novo* (Figure S2) and crossed with *Ucn3-Cre* mice to facilitate

postnatal β-cell deletion without the need for tamoxifen (van der Meulen et al., 2017). Islet PCK2 protein dropped by 67% in the Pck2-βKO compared to Pck2-floxed littermate controls (Figure 1d). None of these knockout mice were glucose intolerant (Figure 1e-g).

The relative contributions of each PK isoform relative to total PK activity was determined in the islet lysates. The endogenous allosteric metabolite, FBP, and pharmacologic PK activators such as TEPP-46 (PKa), have no impact on PKm1 but substantially lower the $K_m$ and raise $V_{max}$ for PKm2 or PKL (Lewandowski et al., 2020). Control islet lysates had a $K_m$ for PEP of ~140 ± 14 μM that did not change significantly in the presence of exogenous FBP ($K_m$, 100 μM ± 10 μM) or PKa ($K_m$, 90 ± 13 μM), while $V_{max}$ increased by about one-third (control, 1.05 ± 0.019 μmol/min; FBP, 1.28 ± 0.006 μmol/min; PKa, 1.36 ± 0.006 μmol/min). Quite remarkably the $V_{max}$ for islet PK activity from PKm1-βKO mice was reduced by 97% compared to controls (Figure 1h), and was too low to estimate $K_m$ accurately. The residual PK remained sensitive to activation by both FBP and PKa and identified a recruitable pool that accounted for only about 10% of the PK activity present in controls islets (Figure 1h), despite compensation from elevated PKm2 protein (Figure 1b). Conversely, β-cell PKm2 deletion lowered islet lysate PK $V_{max}$ by ~20% in the absence of activators, and eliminated both the $K_m$ and $V_{max}$ response to PKa and FBP (Figure 1i), thus ruling out any significant PKL activity. Taken together, mouse islet PK activity is composed of >90% PKm1, with a variable contribution from PKm2 depending on the FBP level, and no discernable contribution from PKL. Given that PKm1 has a low $K_m$, if only considered in terms of total cellular activity (*i.e.* in the absence of any compartmentalized functions), PKm1 should be dominant over PKm2 under all physiologic conditions but especially when the PEP concentration is low.

*PKm1 is sufficient for $K_{ATP}$ channel closure in the plasma membrane microcompartment, while PKm2 requires allosteric activation*

We previously demonstrated that PK, by virtue of its colocalization with $K_{ATP}$ channels, generates a sufficient ATP/ADP ratio to close the channels in mouse and human β-cells even under saturating ADP (Lewandowski et al., 2020). These excised patch-clamp experiments, which expose the inside of the plasma membrane to the bath solution (*i.e.* the inside-out mode), provide both the location of PK as well as its functional coupling to $K_{ATP}$ channels in native β-cell membranes. This approach was re-applied in combination with β-cell deletion of PKm1 and PKm2 to identify the isoforms present in the $K_{ATP}$ microdomain. $K_{ATP}$ channels were identified by inhibition with 1 mM ATP, which blocked the spontaneous opening that occurs after patch excision (Figure 2a). Channel activity was restored using a test solution containing 0.5 mM ADP. In control β-cells, the further addition of 5 mM PEP reduced the total power (a term reflecting both the frequency and channel open time) by 77% in control β-cells (Figure 2a), compared with only a 29% reduction in PKm1-βKO cells (Figure 2b). Note that $K_{ATP}$ channel closure occurred in control β-cells despite the continuous deluge of the channel-opener ADP, which must therefore be locally depleted for $K_{ATP}$ channels to close, placing PK in the $K_{ATP}$ channel microcompartment. Thus, it is not the PEP *per se* but the PK activity in the $K_{ATP}$ microcompartment that is responsible for $K_{ATP}$ closure.

To test for PKm2 in the $K_{ATP}$ microcompartment, PKm1-βKO cells were preincubated in presence of 10 μM PKa, which together with PEP restored $K_{ATP}$ channel closure to control levels with 1 mM ATP alone (Figure 2c). PKa had a similar effect when applied acutely (Figure 2d), indicating that PKm2 does not require allosteric activation to localize to the $K_{ATP}$ microdomain. In addition, since the PEP concentration in the incubations were well over the $K_m$ of either isoform, the response to PKa indicates that channel closure either requires an additional increase in the $V_{max}$ or that the functional interaction is sensitive to the quaternary structure of PKm2 (Figure 2c-d). β-cells lacking PKm2 maintained channel closure without PKa with the same power as 1 mM ATP, which is attributable to the sufficiency of endogenous PKm1 (Figure 2e). Metabolic compartmentation of PKm1 and PKm2 provides enzymatic redundancy as well as a compelling explanation for the ability of PKm1-βKO mice to tolerate a near complete loss of PK activity (Figure 1e,h).

*PKm2 and mitochondrial PEP, but not PKm1, have metabolic control over glucose-stimulated $Ca^{2+}$ oscillations*

The rescue of PKm1 deficiency by PKa in the $K_{ATP}$ microcompartment suggests that PKm1 and PKm2 share local metabolic control over $K_{ATP}$ closure, provided that glucose is available to generate the FBP needed to activate PKm2 (Figure 2c-d). To test this further we examined $Ca^{2+}$ dynamics with FuraRed while using a near-IR dye, DiR, to facilitate simultaneous imaging of PKm1-, PKm2-, and PCK2-βKO islets with their littermate controls (Figure 3a). Indeed, β-cell deletion of PKm1 or PKm2 did not reveal any biologically meaningful differences in the oscillatory period, the fraction of each oscillation spent in the electrically-active state (*i.e.* the duty cycle), or amplitude of glucose-stimulated $Ca^{2+}$ oscillations in intact islets (Figure 3b-c) confirming *in situ* that they are redundant at high glucose. Importantly, the observation that steady-state $Ca^{2+}$ oscillations are normal in PKm1-βKO islets, which retain at maximum only ~10% of PK activity (Figure 1h), indicates that remarkably PK is not kinetically limited (*i.e.* by $V_{max}$) in either the cataplerotic ($Mito_{Cat}$) or oxidative phases ($Mito_{Ox}$) of the oscillation (Figure 3a). It is especially notable then, that the acute application of PKa to normal islets reduced the period as well as the amplitude of the steady-state glucose-induced oscillations (Figure 3d and Figure S3a), indicating significant control by PKm2.

Increasing the glucose concentration will reduce the time spent in the electrically-silent $Mito_{Cat}$ phase of the oscillations (Figure S3b) by accelerating PK-dependent $K_{ATP}$ closure (Figure 2d), while dramatically increasing the fraction of the time spent in the electrically-active $Mito_{Ox}$ phase of the oscillation (i.e. the duty cycle), thereby increasing the oscillatory period (Lewandowski et al., 2020). Interestingly, PKa shortened *both* $Mito_{Cat}$ and $Mito_{Ox}$ to similar extents (Figure S3c) effectively preserving the duty cycle while reducing the period (Figure 3d). These striking observations suggest that, unlike glucose elevation, the PK-driven PEP cycle regulates the onset *and* termination of $Ca^{2+}$ influx. Conversely, in PCK2-βKO islets, both the period and amplitude of glucose-stimulated $Ca^{2+}$ oscillations were increased relative to controls islets (Figure 3e). The period lengthening occurred from increased durations of *both* $Mito_{Cat}$ and

$Mito_{Ox}$ (Figure S3d) and though the duty cycle increased significantly, it was only by a small fraction. This indicates that at a fixed glucose concentration, the "on" and "off" switches arising from PKm2 activation are balanced, and they are substrate-limited by mitochondrial production of PEP.

The above experiments examined conditions at a fixed glucose concentration that may not relate to the transition from low to high glucose where first-phase secretion is observed. Following an acute rise from 2 to 10 mM glucose, PKm1 and PKm2 knockouts had no discernable difference in first-phase $Ca^{2+}$ parameters (i.e., time to depolarization, amplitude, and duration of first phase) (Figure 3f-g). In contrast, addition of PKa to control islets reduced the time to depolarization as well as the duration of the first-phase (Figure 3h). Conversely, depolarization was delayed in Pck2-βKO islets (Figure 3i). However, in this case the duration of the first-phase $Ca^{2+}$ pulse was not calculated since nearly 60% of Pck2-βKO islets failed to exit the first phase plateau in order to begin oscillations, as compared with only 20% of control islets (Figure 3i). That is, while PCK2 knockout had a weaker first phase $Ca^{2+}$ rise, it had a much longer plateau that failed to turn off effectively. So, like the steady-state, PKm2 activation and PCK2 metabolism control $Ca^{2+}$, both serving as on-switches during the triggering phase, $Mito_{Cat}$, and off-switches during the secretory phase, $Mito_{Ox}$.

*Restriction of glycolytic PEP reveals the importance of PCK2 for cytosolic ATP/ADP*

Amino acids (AA) are obligate mitochondrial fuels that simultaneously feed oxidative and anaplerotic pathways. Independent of glycolysis, AA generate PEP via glutamate dehydrogenase (GDH)-mediated anaplerosis that is followed by PCK2-mediated cataplerosis via the mitochondrial GTP cycle (Kibbey et al., 2014; Stark et al., 2009). AA are a tool for separating mechanistic components of the secretion mechanism because at low glucose they raise ATP/ADP but only elicit a single wave of $K_{ATP}$ channel closure, $Ca^{2+}$, and insulin release. We used β-cell specific expression of Perceval-HR biosensors to examine whether restriction of the mitochondrial PEP supply (via PCK2-βKO knockout) impacted the cytosolic ATP/ADP ratio (Gregg et al., 2019, 2016). To limit glycolytic PEP, islets in 2.5 mM glucose were stimulated with a mixture of AA including leucine and glutamine to allosterically activate and fuel GDH, respectively. Consistent with defective PEP cataplerosis, the ATP/ADP response of PCK2-βKO islets was only 37% of control islets in response to AA (Figure 4a), suggesting that the majority of the ATP/ADP increase was PCK2 dependent. In this setting of PCK2 depletion, PK activation did not recover any of the ATP/ADP response (Figure 4b) as expected from the absence of a glycolytic PEP source. Deletion of either PKm1 or PKm2 modestly reduced the β-cell ATP/ADP response to AA (Figure 4c,e), indicating a redundancy for raising ATP/ADP in the absence of glycolytic FBP or PEP. Akin to the patch-clamp studies in Figure 2c-d, PKa completely recovered the PKm1-βKO islets but not the PKm2-βKO islets (Figure 4d,f), indicating that the PKm2 isoform is required for maximal ATP/ADP ratios from AA and that PKm2 is also sufficient in the absence of PKm1. Thus, both PK isoforms redundantly increase the cytosolic ATP/ADP ratio via the PEP cycle. In contrast, PCK2 is essential for amino acids and displays high control strength over ATP/ADP considering that the protein was only reduced by about two-thirds (Figure 1d).

*Pyruvate kinase is essential for $K_{ATP}$ channel closure*

Mitochondria are located throughout the β-cell, including near the plasma membrane, where submembrane ATP microdomains have been observed (Griesche et al., 2019; Kennedy et al., 1999). Since PK is located on the plasma membrane, we wondered whether mitochondria can provide PEP, or alternatively, serve as a direct source of ATP for $K_{ATP}$ channel closure. To determine whether mitochondrial PEP impacts the $K_{ATP}$ channel microcompartment, we monitored $K_{ATP}$ channel currents in *intact* β-cells in the cell-attached configuration in response to bath-applied AA at low glucose (Figure 5a). Mixed AA with or without PKa reduced $K_{ATP}$ channel power (reflecting the total number of transported $K^+$ ions) by ~75% in control β-cells, while the further addition of PKa partially reopened the channel (Figure 5b). No $K_{ATP}$ closure was observed in the absence of PCK2, even with PK activator present (Figure 5c). These findings suggest that mitochondrial PEP is not only capable of signaling to the $K_{ATP}$ channel microcompartment, but is essential for AA-stimulated $K_{ATP}$ closure, and confirm that the mitochondrial anaplerotic/cataplerotic pathway has been isolated from glycolysis with this technique.

Unlike the PCK2-deficient β-cells, PKm1-deficient β-cells stimulated with mitochondrial fuels are capable of increasing cytosolic ATP/ADP to a similar level as controls (Figure 4). This model provides a unique opportunity to determine whether a rise in ATP/ADP in the bulk cytosol is sufficient to close $K_{ATP}$ channels. While control and PKm2-deficient β-cells stimulated with AA effectively closed $K_{ATP}$ channels (Figure 5b and 5d), β-cells from the PKm1-βKO islets failed to do so (Figure 5e). As in excised patches (Figure 2c-d), pharmacologic activation of PKm2 rescued $K_{ATP}$ closure in PKm1-deficient β-cells (Figure 5f). These remarkable findings, by demonstrating that PK activity is essential for $K_{ATP}$ channel closure, argue strongly against a model in which mitochondria raise cytosolic ATP/ADP to close $K_{ATP}$ channels.

*Mitochondrial PEP drives $K_{ATP}$ closure and $Ca^{2+}$ influx during $Mito_{Cat}$, and accelerates $K_{ATP}$ reopening and $Ca^{2+}$ extrusion during $Mito_{Ox}$*

While AA-stimulated $K_{ATP}$ closure does not induce multiple $Ca^{2+}$ oscillations as glucose does, $Ca^{2+}$ influx follows a distinct triggering and recovery phase, representing $Mito_{Cat}$ and $Mito_{Ox}$, respectively (Figure 5g). Following $K_{ATP}$ closure with AA, the channel reopening with PKa (Figure 5b) suggests that PKm2 activation also controls a functionally separable "off" switch that ultimately increases the channel excitability from mitochondrial PEP, which was necessary to switch off $Ca^{2+}$ influx (Figure 3e,i). In other words, PKm2 may switch from an activating function during $Mito_{Cat}$ to an inactivating function during $Mito_{Ox}$, consistent with the ability of PKa to both hasten the onset *and* shorten the duration of $Ca^{2+}$ pulses (Figure 3d,h). To test this concept further, we examined the effect of PKa on AA-stimulated $Ca^{2+}$ influx. When applied early during $Mito_{Cat}$, PKa increased AA-stimulated $Ca^{2+}$ influx (Figure 5h), while PKa application during $Mito_{Ox}$ reduced cytosolic $Ca^{2+}$ (Figure 5i), confirming two temporally separated functions of PKm2 in response to mitochondrial PEP.

*The isoforms of pyruvate kinase, responding to differentially to the glycolytic and mitochondrial sources of PEP, dictate the $Ca^{2+}$ and insulin secretory response to anaplerotic fuels*

We next examined the functional consequence of β-cell PKm1, PKm2, and PCK2 deletion on AA-stimulated $Ca^{2+}$ influx and insulin secretion at both low and high glucose (Figure 6). In intact PCK2-βKO islets at low glucose, like the ATP/ADP ratio (Figure 4a), the AA-induced $Ca^{2+}$ response was reduced along with insulin secretion (Figure 6a,b). Thus, compared to controls, there is a substrate-limited dependency on PCK2 to generate sufficient PEP that is needed to fully engage the secretory apparatus. This dependency on PCK2 was not apparent at 10 mM glucose and reversed by the combination of glucose plus AA compared to controls (Figure 6c). While counterintuitive at first glance, this reversal was expected because of the restored glycolytic PEP supply and the ability of PCK2-deficient β-cells to generate a dysfunctional but sustained $Ca^{2+}$ plateau fraction (Figure 3i). Like the PCK2-βKO, in AA-stimulated islets from PKm1-βKO islets the $Ca^{2+}$ and secretory responses were blunted at low glucose (Figure 6d,e), whereas the insulin secretory response remained intact with glucose (Figure 6f). These findings are entirely consistent with the differential nutrient response of PKm1-dependent $Ca^{2+}$ and $K_{ATP}$ channel closure described above (Figure 3 and 5). The AA secretory response of PKm1-βKO islets was rescued by the presence of glucose (Figure 6f), befitting the recruitment of PKm2 by glycolytic FBP.

Activated PKm2 has complementary functions during $Mito_{Cat}$ and $Mito_{Ox}$ accelerating both $K_{ATP}$ closure and reopening, and consequently, AA-stimulated $Ca^{2+}$ influx and extrusion (Figure 5). Both the AA-induced $Ca^{2+}$ response and insulin secretion were greatly increased in PKm2-βKO islets compared to controls (Figure 6g,h). Glucose alone, but especially in combination with AA, stimulated enhanced secretion in the absence of PKm2 (Figure 6i). While PKm1 is therefore sufficient to initiate secretion during $Mito_{Cat}$, PKm2 is essential for mitochondrial PEP to switch the system off during $Mito_{Ox}$. Thus, when PKm2 is replaced by the constitutively-activated PKm1, the system is shifted towards greater nutrient-induced and, in particular PCK2-dependent, insulin secretion with heightened sensitivity to anaplerotic fuels.

## DISCUSSION

These data provide evidence that PEP has metabolic control over PK-dependent ATP/ADP generation, $K_{ATP}$ closure, $Ca^{2+}$ signaling, and insulin secretion via the PEP cycle. β-cell deletion of PKm1, PKm2, and PCK2 demonstrate that PK is strictly required for $K_{ATP}$ channel closure, and provide a rigorous genetic validation of our hypothesized $Mito_{Cat}$-$Mito_{Ox}$ model of oscillatory metabolism, in which PK is controlled by two sources of PEP – glycolytic and mitochondrial (Figure 1a). During the triggering phase, $Mito_{Cat}$, carbon from either carbohydrate or mitochondrial amino acid metabolism funnels through PCK2 to provide cataplerotic PEP to raise the ATP/ADP ratio in the $K_{ATP}$ channel microcompartment. We show that both PK isoforms are present in the $K_{ATP}$ microenvironment where they regulate channel closure via PEP metabolism. Mitochondrial PEP, generated by PCK2, was further linked to the ability of PKm2 to function as an "off-switch" during $Mito_{Ox}$, when $K_{ATP}$ is reactivated and $Ca^{2+}$ is reduced to reset the oscillatory system.

Our experiments show that a fuel-stimulated rise in the ATP/ADP ratio in the bulk cytosol is insufficient to close $K_{ATP}$ channels, ruling out an important vestige of the "canonical model" in which mitochondria raise cytosolic ATP/ADP to close $K_{ATP}$ channels (Campbell and Newgard,

2021; Prentki et al., 2013; Thompson and Satin, 2021). In PKm1-deficient β-cells, mitochondrial fuels increased the bulk cytosolic ATP/ADP ratio similarly to control β-cells, but were unable to close $K_{ATP}$ channels. Pharmacologic re-activation of PKm2, present on the plasma membrane of PKm1-deficient β-cells, acutely restored $K_{ATP}$ closure. Taken together with the sufficiency of PK for $K_{ATP}$ closure in excised patch experiments, our data support a model in which plasma-membrane compartmentalized PK generates the ATP/ADP ratio to *initiate* insulin secretion, while oxidative phosphorylation plays the dominant role in providing ATP to sustain insulin secretion *after* membrane depolarization (Lewandowski et al., 2020).

In the mouse β-cell, we demonstrate that most of the PK is the constitutively-active PKm1 isoform, with a minor contribution from PKm2 and no detectable PKL activity. In the rat, MacDonald and Chang (MacDonald and Chang, 1985) reported PK activity to be primarily PKm2, which may be a species difference and/or an overestimation of the FBP responsivity which was modest. Our prior studies of PK-dependent $K_{ATP}$ closure in human β-cell plasma membranes were conducted in the absence of FBP, which is consistent with the presence of PKm1 in the microdomain but not ruling out PKm2 (Lewandowski et al., 2020). Regardless, PKm2 activators amplify nutrient-stimulated insulin secretion in mouse, rat, and human islets in vitro, and in rats in vivo, indicating that PKm2 is functionally recruitable in all three species (Abulizi et al., 2020; Lewandowski et al., 2020).

Paradoxically, PKm2 has metabolic control over glucose-dependent $K_{ATP}$ closure even though PKm2 deletion had no effect on first-phase or steady-state $Ca^{2+}$ oscillations. This occurs because $K_{ATP}$ closure is not kinetically limited by PK activity (i.e. by $V_{max}$) at any point in the oscillatory cycle. The PKm1-βKO, which has >90% loss of islet PK activity and no defect in $Ca^{2+}$ oscillations, makes this point especially clear. If mitochondrially-derived ATP/ADP was limiting for $K_{ATP}$ closure, it would have been observed here. Consistently, a substantial loss of oxidative phosphorylation is not necessarily accompanied by perturbations in $Ca^{2+}$ oscillations (Gregg et al., 2019) or insulin secretion (Fu et al., 2009). We conclude that electron transport chain inhibitors prevent $K_{ATP}$ closure (Gregg et al., 2019) because they slow glycolysis. From the excised patch-experiments, we learned that PKm2 requires allosteric activation to close $K_{ATP}$ channels. While the precise mechanism is unknown, FBP allows PKm2, but not PKm1, to transmit the signal from glucose to the $K_{ATP}$ channel. Nonetheless, both PK enzymes are sensitive to the level of PEP. Amino acids, as anaplerotic mitochondrial fuels, can generate mitochondrial PEP but do not generate FBP, which explains how shifting the β-cell from PKm2 to PKm1 increases the secretory response to anaplerotic fuels.

Whole-body $PCK2^{-/-}$ mice display glucose intolerance and reduced insulin secretion (Abulizi et al., 2020). These effects may arise during development or independently of the β-cell, since PCK2-βKO mice of a similar age are glucose tolerant and display increased insulin secretion from isolated islets. Nevertheless, $Ca^{2+}$ influx induced by amino acid stimulation is blocked in both models, and we further demonstrated that PCK2 is rate controlling for cytosolic ATP/ADP generation and $K_{ATP}$ closure. Befitting the importance of the PEP cycle under physiological or high glucose conditions, β-cell deletion of PCK2 had a strong effect on glucose-stimulated $Ca^{2+}$

oscillations, delaying both the onset of $Ca^{2+}$ influx and the ability of β-cells to repolarize. The failure of this off-switch explains the hypersecretion in the β-cells lacking PCK2 when anaplerosis is fully primed with glucose and amino acids.

Insulin release is frequently described in terms of triggering and amplifying on-signals termed "metabolic coupling factors" (MCFs). As defined by Prentki, "regulatory MCFs" are nutrient-dependent signals that facilitate the switch between metabolic networks (e.g. malonyl-CoA switches β-cells from fatty acid to glucose oxidation), while "effectory MCFs" (e.g., $Ca^{2+}$, ATP/ADP, monoacylglycerol, and reactive oxygen species), are transient, necessary, and sufficient on-signals that dose-dependently stimulate insulin secretion (Prentki et al., 2013). Is PEP a regulatory or effectory signal for insulin secretion – or both? PEP has some properties of a regulatory signal, since its metabolism by PK generates a bioenergetic feed forward that progressively deprives mitochondria of ADP, shutting down oxidative phosphorylation in favor of activating both pyruvate carboxylase and the PEP cycle (Lewandowski et al., 2020; Sugden and Ashcroft, 1977). Through a positive Hill coefficient, as the PEP concentration rises, it progressively activates PKm2 to make more ATP (Lewandowski et al., 2020; Merrins et al., 2013), further reinforcing the PEP cycle. Arguably, PEP also has effectory properties, since its presence in the $K_{ATP}$ microenvironment in the excised patches can override channel opening by continuous ADP to close $K_{ATP}$ channels. This property requires either PKm1 or allosterically-activated PKm2. Likewise, in intact cells exposed to amino acids, PCK2-derived PEP was rate limiting to block $K_{ATP}$ through a process independent of the bulk cytosolic ATP/ADP ratio. The ATP/ADP ratio at the plasma membrane is clearly effectory in that it is sufficient to cause depolarization (Ashcroft et al., 1984; Cook and Hales, 1984; Rorsman and Trube, 1985) while at the same time priming granule exocytosis (Eliasson et al., 1997; Pizarro-Delgado et al., 2016; Takahashi et al., 1999). Assigning PEP an effectory role based on its essentiality and sufficiency would nevertheless be hasty as we do not yet know whether it dose-dependently increases exocytosis.

Effectory MCFs must be counterbalanced by a strong off-switch that ensures the signal is transient. That is, β-cells can fail if $K_{ATP}$-dependent $Ca^{2+}$ influx is activated without a coordinated homeostatic mechanism to turn it off (Remedi and Nichols, 2009). While PKm2 activation during $Mito_{Cat}$ was found to facilitate $K_{ATP}$ closure and increase $Ca^{2+}$, we also found that PKm2 accelerated $K_{ATP}$ channel reopening and lowered $Ca^{2+}$ during $Mito_{Ox}$. Like the on-switch, this off-switch may also involve mitochondrial PEP, since β-cell PCK2 deletion stalls the system in the $Ca^{2+}$-activated state. Spatial considerations, such as the stimulus-dependent movement of the mitochondria away from the plasma membrane (Griesche et al., 2019), may also contribute to $Ca^{2+}$ cycling. Further studies are needed to elucidate the understudied homeostatic functions of PKm2 and mitochondrial PEP, and may help to explain how overnutrition perturbs β-cell function in diabetes.

## ACKNOWLEDGEMENTS

We would like to thank Matthew Vander Heiden (MIT) for providing PKm1$^{f/f}$ mice, and Mark Huising (UC-Davis) and Barak Blum (UW-Madison) for providing Ucn3-Cre mice. We would also like to acknowledge Kathy Krentz and Dustin Rubenstein at the UW-Madison Genome Editing and Animal Model Core for their assistance generating PCK2$^{f/f}$ mice, and Jiwon Seo and Jody Peter at the UW-Madison Biomedical Research Model Services Breeding Core for their assistance with animal husbandry and genotyping. The Merrins laboratory gratefully acknowledges support from the NIH/NIDDK (R01DK113103 and R01DK113103) and the Department of Veterans Affairs (I01B005113). HRF received a postdoctoral fellowships from HRSA (T32HP10010) and the NIH/NIA (T32AG000213), SLL received a predoctoral fellowship from the NIH/NIDDK (T32DK007665), HRV received a postdoctoral fellowship from the American Diabetes Association (1-17-PDF-155), and we acknowledge Dudley Lamming for contributing support for EP from R01AG062328. The Kibbey laboratory gratefully acknowledges support from the NIH/NIDDK (R01DK127637). This work utilized facilities and resources from the William S. Middleton Memorial Veterans Hospital and does not represent the views of the Department of Veterans Affairs or the United States Government.

## AUTHOR CONTRIBUTIONS

MJM conceived the study and wrote the paper with HRF and RGK. HRF performed the main body of the experiments with assistance from TH, EP, SMS, SLL, HRV, SMD, and RLC. MJM and RGK provided resources. All authors interpreted the data and edited the manuscript.

## DECLARATION OF INTERESTS

The authors declare no competing interests.

## MATERIALS AND METHODS

### *Mice Creation*

β-cell specific PKm1 and PKm2 knockout mice were generated by breeding *Ins1-Cre* (Thorens et al., 2015) mice (B6(Cg)-*Ins1*$^{tm1.1(cre)Thor}$/*J*, Jackson Laboratory #026801) with *Pkm1*$^{f/f}$ mice (Davidson et al., 2021; Li et al., 2021, p. 1) provided by Matthew Vander Heiden (MIT) or *Pkm2*$^{f/f}$ mice (Israelsen et al., 2013) (B6;129S-*Pkm*$^{tm1.1Mgvh}$/J, Jackson Laboratory #024408) after 10 generations of backcrossing to C57BL6/J mice (Jackson Laboratory). *Pck2*$^{f/f}$ mice were generated *de novo* by the University of Wisconsin-Madison Genome Editing and Animal Model core. Backcrossed F1s were sequence confirmed by Illumina targeted deep sequencing to confirm the LoxP insertions around exon 5 (ENSMUSE00000399990; Figure S1), and the intervening region was sequence confirmed with Sanger sequencing. *Pck2*$^{f/f}$ mice were crossed with *Ucn3-Cre* mice (van der Meulen et al., 2017) provided by Barak Blum (University of Wisconsin-Madison) with permission from Mark O. Huising (University of California-Davis). All mice were genotyped by Transnetyx.

*Mouse Islet Preparations*

Male mice were housed 2-5 per cage at 21-23°C, fed with a chow diet and water provided *ad libitum*, and maintained on a 12 h light/dark cycle. Mice 12-20 weeks of age were sacrificed via $CO_2$ asphyxiation followed by cervical dislocation, and islets were isolated using methods previously described (Gregg et al., 2016).

*Cloning and Adenoviral Delivery of Biosensors*

Generation of adenovirus carrying genetically-encoded ATP/ADP biosensors (Perceval-HR) under control of the insulin promoter was described previously (Merrins et al., 2016). High-titer adenovirus was added to islets immediately after islet isolation and incubated for 2 h at 37°C then moved to fresh media. Imaging was performed 3 days post isolation.

*Western blots*

Islets were lysed using 0.1% Triton-X100 in phosphate buffered saline (1 µl/islet). Islets in lysis buffer were incubated at room temperature for 15 minutes, vortexed for 30 seconds, frozen/thawed, and vortexed for 30 seconds again. Cell lysate was spun down at max speed in a table top centrifuge and 16-20 µl supernatant was added to each well of a 12% SDS-PAGE gel. The gel was run at 110V for ~2 hours then transferred to a PVDF membrane at 100V for 1 hour at 4°C. Membranes were blocked in 4% BSA in Tris-buffered saline containing 0.1% Tween-20 detergent (TBST) for 30 minutes then incubated overnight with PKm1 (Cell Signaling #4053; 1:1000), PKm2 (Cell Signaling #7067; 1:1000), PCK2 primary antibodies (Cell Signaling #6924; 1:1000), or loading controls beta-actin (Cell Signaling #3700; 1:1000) or HSP90 (Cell Signaling #4877; 1:1000). Blots were washed for 15 min in TBST four times then incubated for 2 hours at room temperature with an anti-rabbit IgG HRP-linked secondary antibody (Cell Signaling #7074; 1:20,000). Blots were imaged and quantified using ImageQuant (Amersham).

*Timelapse Imaging*

Islets were preincubated in 2.5 µM FuraRed (Molecular Probes F3020) in RPMI 1640 for 45 minutes at 37°C prior to being placed in an glass-bottomed imaging chamber (Warner Instruments) on a Nikon Eclipse Ti-E inverted microscope with a Super Flour 10x/0.5N.A. objective (Nikon Instruments). The chamber was perfused with standard imaging solution (in mM: 135 NaCl, 4.8 KCl, 5 $CaCl_2$, 20 HEPES, 1.2 $MgCl_2$) for low glucose/amino acid experiments, or HBSS (in mM 137 NaCl, 5.6 KCl, 1.2 $MgCl_2$, 0.5 $NaH_2PO_4$, 4.2 $NaHCO_3$, 10 HEPES, 2.6 $CaCl_2$) for high glucose experiments containing glucose and amino acid concentrations indicated in figure legends. Temperature was maintained at 33°C with inline solution and chamber heaters (Warner Instruments), and flow rate was set to 0.25 ml/min. Excitation was provided by a SOLA SE II 365 (Lumencor). A Hamamatsu ORCA-Flash4.0 V2 Digital CMOS camera was used to collect fluorescence emission at 0.125-0.2 Hz. Nikon NIS-Elements was used to designate regions of interest. Excitation (x) and emission (m) filters (ET type; Chroma Technology) were used with an FF444/521/608-Di01 dichroic (Semrock) as follows: FuraRed, 430/20x and 500/20x, 630/70m

(R430/500 was reported) and Perceval-HR, 430/20x and 500/20x, 535/35m (R500/430 was reported). A custom MATLAB script was used to quantify cytosolic $Ca^{2+}$ oscillation parameters. In order to differentiate between islets of control and knockout mice, islets of one genotype were barcoded by pre-incubation with 2 µM DiR (Fisher Scientific D12731) or 2 µM DiD (Fisher Scientific D7757) in islet media for 10 minutes at 37°C. Islet barcodes were then imaged using a Cy7 (for DiR) or Cy5 filter cube (for DiD) from Chroma.

*Electrophysiology*

Single channel patch clamp experiments and data analysis were performed as previously described (Lewandowski et al., 2020). Briefly, mouse and human cells were acutely isolated by dispersing of islets with Accutase (Fisher Scientific). Cells were plated on sterilized uncoated glass shards and kept at 37ºC with 95% $O_2$-5% $CO_2$. For both on-cell and inside-out recordings, gigaseals were obtained in extracellular bath solution (in mM): 140 NaCl, 5 KCl, 1.2 $MgCl_2$, 2.5 $CaCl_2$, 0.5 Glucose, 10 HEPES, pH 7.4, adjusted with NaOH and clamped at −50mV. For inside-out configuration, after pipette excision, the bath solution was replaced with equilibrium solutions with $K^+$ as the charge carrier (in mM): 130 KCl, 2 $CaCl_2$, 10 EGTA, 0.9 $[Mg^{2+}]_{free}$, 10 sucrose, 20 HEPES, pH 7.2 with KOH. The $[Mg^{2+}]_{free}$, calculated using WEBMAXC standard, was held constant in the presence of nucleotides. The pipette solution, used for both on-cell and inside-out configurations, contained (in mM): 10 sucrose, 130 KCl, 2 $CaCl_2$, 10 EGTA, 20 HEPES, pH 7.2, adjusted with KOH. Recording electrodes made of microfilament borosilicate glass (Harvard Apparatus, Holliston, MA #64-0792) were used to pull patch pipettes (3 MΩ) on a horizontal Flaming/Brown micropipette puller (P-1000, Sutter Instruments) and polished by microforge (Narishige MF-830) to a final tip resistance of 5-10 MΩ. On-cell recording started after formation of a stable gigaseal (>2.5 GΩ) and inside-out recording started after withdrawal of the pipette and establishment of the excised inside-out configuration. A HEKA Instruments EPC10 patch-clamp amplifier was used for registration of current. Data was Bessel filtered online at 1 kHz and single channel currents were analyzed offline using ClampFit analysis module of pCLAMP 10 software (Molecular Devices).

*Islet Perifusion Assays*

Islets from 6 mice of each genotype were pooled and then divided in equal numbers and placed into a 12-channel perifusion system (BioRep Peri-4.2; 75-100 islets/chamber) containing KRPH buffer (in mM: 140 NaCl, 4.7 KCl, 1.5 $CaCl_2$, 1 $NaH_2PO_4$, 1 $MgSO_4$, 2 $NaHCO_3$, 5 HEPES, 2 glucose, 0.1% fatty acid-free BSA, pH 7.4) with 100 µl Bio-Gel P-4 Media (Bio-Rad). Islets were equilibrated at 2 mM glucose for 36-48 minutes prior to perfusion with amino acids or 10 mM glucose at 37ºC. Insulin secretion was assayed using Promega Lumit™ Insulin Immunoassay (CS3037A01) and measured using a TECAN Spark plate reader. Quant-IT PicoGreen dsDNA Assay Kit (Thermo Scientific P7589) was used to determine DNA content after lysis using 0.1% Triton X-100.

*PK activity*

The enzymatic activity of pyruvate kinase was measured using EC 2.7.1.40 from Sigma (Bergmeyer, H.U. et al., n.d.) as described previously (Lewandowski et al., 2020). FBP (Sigma Aldrich #F6803) and TEPP-46 (PKa; Fisher Scientific #50-548-70001) were used at a concentration of 80 µM and 10 µM, respectively. Experiments were performed at 37ºC.

*Quantification and Statistical Analysis*

Figure legends describe the statistical details of each experiments. Data are expressed as mean ± SEM. Statistical significance was determined by two-way or one-way ANOVA with Sidak multiple-comparisons test post hoc or Student's t-test as indicated in the figure legends. Data were continuous and normally distributed so were analyzed with parametric tests. Differences were considered to be significant at $P < 0.05$. Calculations were performed using GraphPad Prism.

*Study approval*

Animal experiments were conducted under the supervision of the IACUC of the William S. Middleton Memorial Veterans Hospital (Protocol: MJM0001).

## REFERENCES


Abulizi A, Cardone RL, Stark R, Lewandowski SL, Zhao X, Hillion J, Ma L, Sehgal R, Alves TC, Thomas C, Kung C, Wang B, Siebel S, Andrews ZB, Mason GF, Rinehart J, Merrins MJ, Kibbey RG. 2020. Multi-Tissue Acceleration of the Mitochondrial Phosphoenolpyruvate Cycle Improves Whole-Body Metabolic Health. *Cell Metab* **32**:751-766.e11. doi:10.1016/j.cmet.2020.10.006

Anastasiou D, Yu Y, Israelsen WJ, Jiang J-K, Boxer MB, Hong BS, Tempel W, Dimov S, Shen M, Jha A, Yang H, Mattaini KR, Metallo CM, Fiske BP, Courtney KD, Malstrom S, Khan TM, Kung C, Skoumbourdis AP, Veith H, Southall N, Walsh MJ, Brimacombe KR, Leister W, Lunt SY, Johnson ZR, Yen KE, Kunii K, Davidson SM, Christofk HR, Austin CP, Inglese J, Harris MH, Asara JM, Stephanopoulos G, Salituro FG, Jin S, Dang L, Auld DS, Park H-W, Cantley LC, Thomas CJ, Vander Heiden MG. 2012. Pyruvate kinase M2 activators promote tetramer formation and suppress tumorigenesis. *Nat Chem Biol* **8**:839–847. doi:10.1038/nchembio.1060

Anderson E, Long JA. 1947. The effect of hyperglycemia on insulin secretion as determined with the isolated rat pancreas in a perfusion apparatus. *Endocrinology* **40**:92–97. doi:10.1210/endo-40-2-92

Ashcroft FM, Harrison DE, Ashcroft SJ. 1984. Glucose induces closure of single potassium channels in isolated rat pancreatic beta-cells. *Nature* **312**:446–448.

Bergmeyer, H.U., Gawehn, K., Grassl, M. n.d. Methods of Enzymatic Analysis. New York, NY: Academic Press, Inc. pp. 5109–510.

Campbell JE, Newgard CB. 2021. Mechanisms controlling pancreatic islet cell function in insulin secretion. *Nat Rev Mol Cell Biol* **22**:142–158. doi:10.1038/s41580-020-00317-7

Cochrane VA, Yang Z, Dell'Acqua ML, Shyng S-L. 2021. AKAP79/150 coordinates leptin-induced PKA signaling to regulate KATP channel trafficking in pancreatic β-cells. *J Biol Chem* **296**:100442. doi:10.1016/j.jbc.2021.100442

Cook DL, Hales CN. 1984. Intracellular ATP directly blocks K+ channels in pancreatic B-cells. *Nature* **311**:271–273. doi:10.1038/311271a0

Corkey BE. 2020. Targeting Pyruvate Kinase PEPs Up Insulin Secretion and Improves Glucose Homeostasis. *Cell Metab* **32**:693–694. doi:10.1016/j.cmet.2020.10.008

Davidson SM, Heyman JE, O'Brien JP, Liu AC, Schmidt DR, Israelsen WJ, Dayton TL, Sehgal R, Bronson RT, Freinkman E, Mak H, Malstrom S, Bellinger G, Carracedo A, Pandolfi PP, Courtney KD, Jha A, DePinho RA, Horner JW, Thomas CJ, Cantley LC, Loda M, Heiden MGV. 2021. Pyruvate kinase M1 suppresses development and progression of prostate adenocarcinoma. doi:10.1101/2021.05.09.443334

DiGruccio MR, Mawla AM, Donaldson CJ, Noguchi GM, Vaughan J, Cowing-Zitron C, van der Meulen T, Huising MO. 2016. Comprehensive alpha, beta and delta cell transcriptomes reveal that ghrelin selectively activates delta cells and promotes somatostatin release from pancreatic islets. *Mol Metab* **5**:449–458. doi:10.1016/j.molmet.2016.04.007

Eliasson L, Renström E, Ding WG, Proks P, Rorsman P. 1997. Rapid ATP-dependent priming of secretory granules precedes Ca(2+)-induced exocytosis in mouse pancreatic B-cells. *J Physiol (Lond)* **503 ( Pt 2)**:399–412. doi:10.1111/j.1469-7793.1997.399bh.x

Fu A, Ng AC-H, Depatie C, Wijesekara N, He Y, Wang G-S, Bardeesy N, Scott FW, Touyz RM, Wheeler MB, Screaton RA. 2009. Loss of Lkb1 in adult beta cells increases beta cell mass and enhances glucose tolerance in mice. *Cell Metab* **10**:285–295. doi:10.1016/j.cmet.2009.08.008

Gregg T, Poudel C, Schmidt BA, Dhillon RS, Sdao SM, Truchan NA, Baar EL, Fernandez LA, Denu JM, Eliceiri KW, Rogers JD, Kimple ME, Lamming DW, Merrins MJ. 2016. Pancreatic β-Cells From Mice Offset Age-Associated Mitochondrial Deficiency With Reduced KATP Channel Activity. *Diabetes* **65**:2700–2710. doi:10.2337/db16-0432

Gregg T, Sdao SM, Dhillon RS, Rensvold JW, Lewandowski SL, Pagliarini DJ, Denu JM, Merrins MJ. 2019. Obesity-dependent CDK1 signaling stimulates mitochondrial respiration at complex I in pancreatic β-cells. *J Biol Chem* **294**:4656–4666. doi:10.1074/jbc.RA118.006085

Griesche N, Sanchez G, Hermans C, Idevall-Hagren O. 2019. Cortical mitochondria regulate insulin secretion by local Ca2+ buffering in rodent beta cells. *J Cell Sci* **132**:jcs228544. doi:10.1242/jcs.228544

Grodsky GM, Batts AA, Bennett LL, Vcella C, Mcwilliams NB, Smith DF. 1963. EFFECTS OF CARBOHYDRATES ON SECRETION OF INSULIN FROM ISOLATED RAT PANCREAS. *Am J Physiol* **205**:638–644. doi:10.1152/ajplegacy.1963.205.4.638

Israelsen WJ, Dayton TL, Davidson SM, Fiske BP, Hosios AM, Bellinger G, Li J, Yu Y, Sasaki M, Horner JW, Burga LN, Xie J, Jurczak MJ, DePinho RA, Clish CB, Jacks T, Kibbey RG, Wulf GM, Di Vizio D, Mills GB, Cantley LC, Vander Heiden MG. 2013. PKM2 isoform-specific deletion reveals a differential requirement for pyruvate kinase in tumor cells. *Cell* **155**:397–409. doi:10.1016/j.cell.2013.09.025

Jesinkey SR, Madiraju AK, Alves TC, Yarborough OH, Cardone RL, Zhao X, Parsaei Y, Nasiri AR, Butrico G, Liu X, Molina AJ, Rountree AM, Neal AS, Wolf DM, Sterpka J, Philbrick WM, Sweet IR, Shirihai OH, Kibbey RG. 2019. Mitochondrial GTP Links Nutrient Sensing to β Cell Health, Mitochondrial Morphology, and Insulin Secretion Independent of OxPhos. *Cell Rep* **28**:759-772.e10. doi:10.1016/j.celrep.2019.06.058

Kennedy HJ, Pouli AE, Ainscow EK, Jouaville LS, Rizzuto R, Rutter GA. 1999. Glucose generates sub-plasma membrane ATP microdomains in single islet beta-cells. Potential role for strategically located mitochondria. *J Biol Chem* **274**:13281–13291.

Kibbey RG, Choi CS, Lee H-Y, Cabrera O, Pongratz RL, Zhao X, Birkenfeld AL, Li C, Berggren P-O, Stanley C, Shulman GI. 2014. Mitochondrial GTP insensitivity contributes to hypoglycemia in hyperinsulinemia hyperammonemia by inhibiting glucagon release. *Diabetes* **63**:4218–4229. doi:10.2337/db14-0783

Lewandowski SL, Cardone RL, Foster HR, Ho T, Potapenko E, Poudel C, VanDeusen HR, Sdao SM, Alves TC, Zhao X, Capozzi ME, de Souza AH, Jahan I, Thomas CJ, Nunemaker CS, Davis DB, Campbell JE, Kibbey RG, Merrins MJ. 2020. Pyruvate Kinase Controls Signal Strength in the Insulin Secretory Pathway. *Cell Metab* **32**:736-750.e5. doi:10.1016/j.cmet.2020.10.007

Li Q, Li C, Elnwasany A, Sharma G, An YA, Zhang G, Elhelaly WM, Lin J, Gong Y, Chen G, Wang M, Zhao S, Dai C, Smart CD, Liu J, Luo X, Deng Y, Tan L, Lv S-J, Davidson SM, Locasale JW, Lorenzi PL, Malloy CR, Gillette TG, Vander Heiden MG, Scherer PE, Szweda LI, Fu G, Wang ZV. 2021. PKM1 Exerts Critical Roles in Cardiac Remodeling Under Pressure Overload in the Heart. *Circulation* **144**:712–727. doi:10.1161/CIRCULATIONAHA.121.054885

MacDonald MJ, Chang CM. 1985. Pancreatic islets contain the M2 isoenzyme of pyruvate kinase. Its phosphorylation has no effect on enzyme activity. *Mol Cell Biochem* **68**:115–120. doi:10.1007/bf00219375

Merrins MJ, Poudel C, McKenna JP, Ha J, Sherman A, Bertram R, Satin LS. 2016. Phase Analysis of Metabolic Oscillations and Membrane Potential in Pancreatic Islet β-Cells. *Biophys J* **110**:691–699. doi:10.1016/j.bpj.2015.12.029

Merrins MJ, Van Dyke AR, Mapp AK, Rizzo MA, Satin LS. 2013. Direct measurements of oscillatory glycolysis in pancreatic islet β-cells using novel fluorescence resonance energy transfer (FRET) biosensors for pyruvate kinase M2 activity. *J Biol Chem* **288**:33312–33322. doi:10.1074/jbc.M113.508127

Mitok KA, Freiberger EC, Schueler KL, Rabaglia ME, Stapleton DS, Kwiecien NW, Malec PA, Hebert AS, Broman AT, Kennedy RT, Keller MP, Coon JJ, Attie AD. 2018. Islet proteomics reveals genetic variation in dopamine production resulting in altered insulin secretion. *J Biol Chem* **293**:5860–5877. doi:10.1074/jbc.RA117.001102

Nicholls DG. 2016. The Pancreatic β-Cell: A Bioenergetic Perspective. *Physiol Rev* **96**:1385–1447. doi:10.1152/physrev.00009.2016

Pizarro-Delgado J, Deeney JT, Corkey BE, Tamarit-Rodriguez J. 2016. Direct Stimulation of Islet Insulin Secretion by Glycolytic and Mitochondrial Metabolites in KCl-Depolarized Islets. *PLoS ONE* **11**:e0166111. doi:10.1371/journal.pone.0166111

Prentki M, Matschinsky FM, Madiraju SRM. 2013. Metabolic signaling in fuel-induced insulin secretion. *Cell Metab* **18**:162–185. doi:10.1016/j.cmet.2013.05.018

Remedi MS, Nichols CG. 2009. Hyperinsulinism and diabetes: genetic dissection of beta cell metabolism-excitation coupling in mice. *Cell Metab* **10**:442–453. doi:10.1016/j.cmet.2009.10.011

Rorsman P, Trube G. 1985. Glucose dependent K+-channels in pancreatic beta-cells are regulated by intracellular ATP. *Pflugers Arch* **405**:305–309.

Stark R, Pasquel F, Turcu A, Pongratz RL, Roden M, Cline GW, Shulman GI, Kibbey RG. 2009. Phosphoenolpyruvate cycling via mitochondrial phosphoenolpyruvate carboxykinase

links anaplerosis and mitochondrial GTP with insulin secretion. *J Biol Chem* **284**:26578–26590. doi:10.1074/jbc.M109.011775

Sugden MC, Ashcroft SJ. 1977. Phosphoenolpyruvate in rat pancreatic islets: a possible intracellular trigger of insulin release? *Diabetologia* **13**:481–486. doi:10.1007/BF01234500

Takahashi N, Kadowaki T, Yazaki Y, Ellis-Davies GC, Miyashita Y, Kasai H. 1999. Post-priming actions of ATP on Ca2+-dependent exocytosis in pancreatic beta cells. *Proc Natl Acad Sci USA* **96**:760–765. doi:10.1073/pnas.96.2.760

Thompson B, Satin LS. 2021. Beta-Cell Ion Channels and Their Role in Regulating Insulin Secretion. *Compr Physiol* **11**:1–21. doi:10.1002/cphy.c210004

Thorens B, Tarussio D, Maestro MA, Rovira M, Heikkilä E, Ferrer J. 2015. Ins1(Cre) knock-in mice for beta cell-specific gene recombination. *Diabetologia* **58**:558–565. doi:10.1007/s00125-014-3468-5

van der Meulen T, Mawla AM, DiGruccio MR, Adams MW, Nies V, Dólleman S, Liu S, Ackermann AM, Cáceres E, Hunter AE, Kaestner KH, Donaldson CJ, Huising MO. 2017. Virgin Beta Cells Persist throughout Life at a Neogenic Niche within Pancreatic Islets. *Cell Metab* **25**:911-926.e6. doi:10.1016/j.cmet.2017.03.017

Figure 1

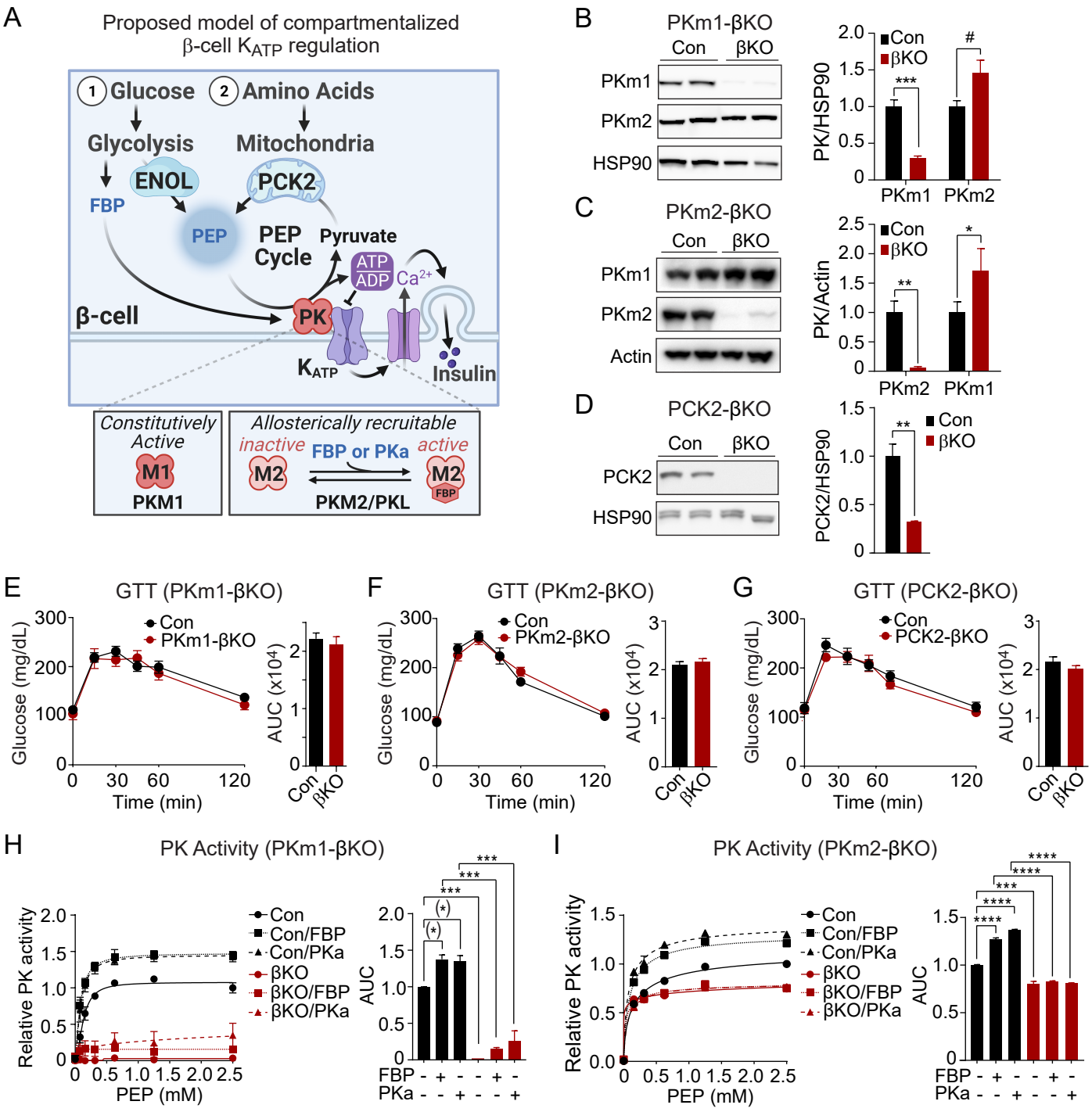
A
Proposed model of compartmentalized β-cell KATP regulation
1 Glucose
2 Amino Acids
Glycolysis
Mitochondria
ENOL
PCK2
FBP
PEP
PEP Cycle
Pyruvate
ATP
ADP
Ca2+
β-cell
PK
KATP
Insulin
Constitutively Active
M1
PKM1
Allosterically recruitable
inactive
FBP or PKa
active
M2
M2
FBP
PKM2/PKL
B
PKm1-βKO
Con
βKO
PKm1
PKm2
HSP90
PK/HSP90
Con
βKO
***
#
PKm1
PKm2
C
PKm2-βKO
Con
βKO
PKm1
PKm2
Actin
PK/Actin
**
*
PKm2
PKm1
D
PCK2-βKO
Con
βKO
PCK2
HSP90
PCK2/HSP90
**
E
GTT (PKm1-βKO)
Con
PKm1-βKO
Glucose (mg/dL)
Time (min)
AUC (x10⁴)
F
GTT (PKm2-βKO)
Con
PKm2-βKO
G
GTT (PCK2-βKO)
Con
PCK2-βKO
H
PK Activity (PKm1-βKO)
Relative PK activity
PEP (mM)
Con
Con/FBP
Con/PKa
βKO
βKO/FBP
βKO/PKa
AUC
FBP
PKa
I
PK Activity (PKm2-βKO)
Relative PK activity
PEP (mM)
AUC
FBP
PKa

**Figure 1. Generation of mouse models to probe the functions of PKm1, PKm2, and PCK2 in β-cells.**

(A) Hypothesized model in which PK in the $K_{ATP}$ microcompartment is fueled by two sources of PEP—glycolytic PEP generated by enolase, and mitochondrial PEP generated by PCK2 in response to anaplerotic fuels. β-cells express three isoforms of PK, constitutively active PKm1 and allosterically recruitable PKm2 and PKL that are activated by endogenous fructose 1,6-bisphosphate (FBP) or pharmacologic PK activators (PKa).

(B-D) Quantification of knockdown efficiency in islet lysates from PKm1-βKO (B), PKm2-βKO (C), and Pck2-βKO mice (D) ($n$ = 4 mice for PKm1- and PCK2-βKO, $n$ = 6 mice for PKm2-βKO).

(E-G) Intraperitoneal glucose tolerance tests (GTT, 1 g/kg) of PKm1-βKO mice ($n$ = 9) and littermate controls ($n$ = 8) (E), PKm2-βKO mice ($n$ = 7) and littermate controls ($n$ = 7) (F), and Pck2-βKO mice ($n$ = 10) and littermate controls ($n$ = 7) (G) following an overnight fast.

(H-I) PK activity in islet lysates of PKm1-βKO (H) and PKm2-βKO mice (I) in response to FBP (80 µM) and PKa (10 µM TEPP-46). ($n$ = 2 replicates from 6 mice/group)

Data are shown as mean ± SEM. $^{\#}P < 0.01$, $^{*}P < 0.05$, $^{**}P < 0.01$, $^{***}P < 0.001$, $^{****}P < 0.0001$ by t-test (B-G) or two-way ANOVA (H-I).

# Figure 2

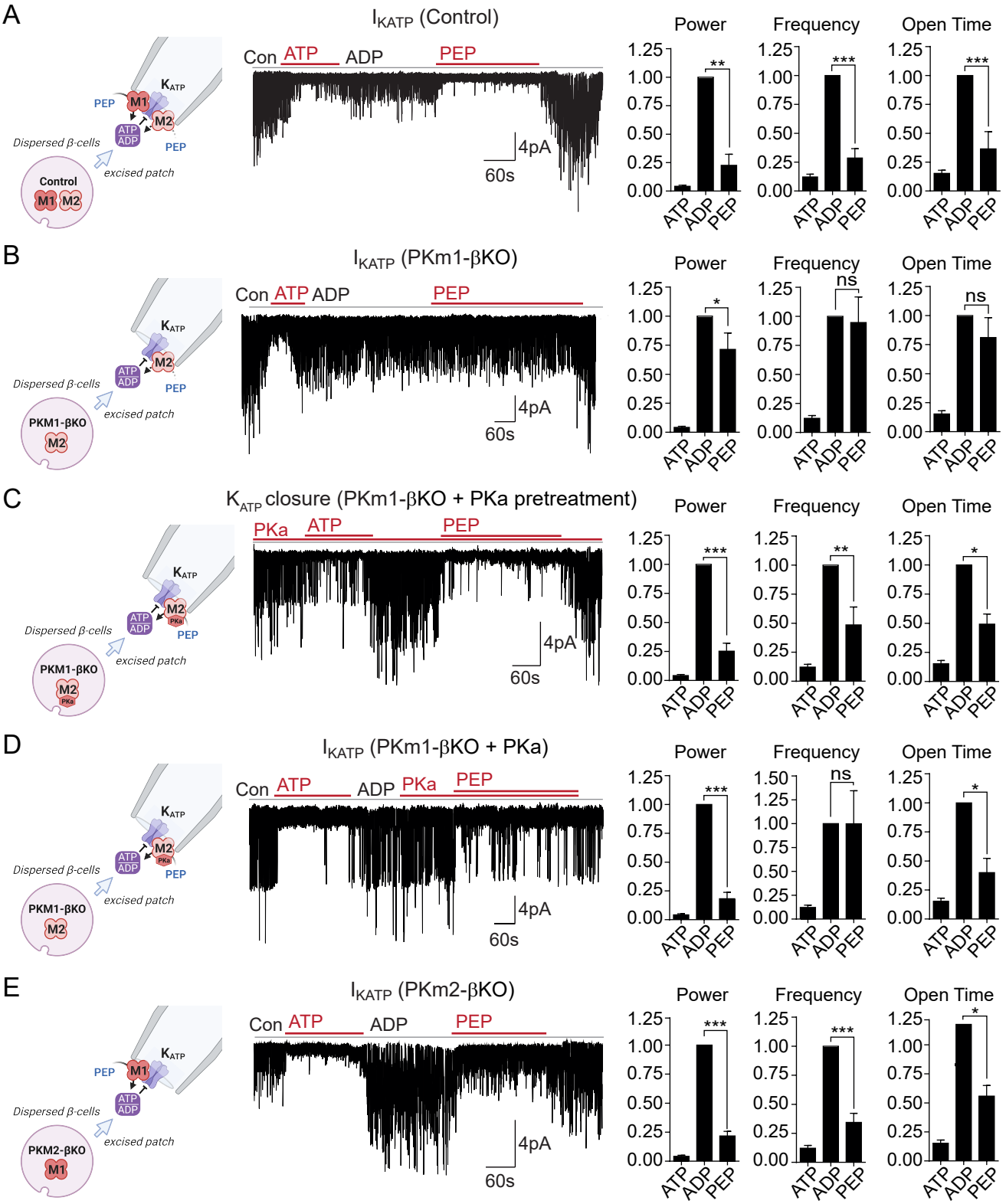

A
$I_{KATP}$ (Control)
Con ATP ADP PEP
4pA
60s
Power
Frequency
Open Time
ATP ADP PEP
Dispersed β-cells
excised patch
Control
M1 M2
B
$I_{KATP}$ (PKm1-βKO)
Con ATP ADP PEP
PKM1-βKO
C
$K_{ATP}$ closure (PKm1-βKO + PKa pretreatment)
PKa ATP PEP
D
$I_{KATP}$ (PKm1-βKO + PKa)
Con ATP ADP PKa PEP
E
$I_{KATP}$ (PKm2-βKO)
Con ATP ADP PEP
PKM2-βKO

**Figure 2. Plasma membrane $K_{ATP}$ channels are locally regulated by a combination of PKm1 and allosterically activated PKm2.**

(A-E) $K_{ATP}$ channel activity (holding potential = -50 mV) quantified in terms of power, frequency, and open time. Applying the substrates for PK closes $K_{ATP}$ channels in excised patches of β-cell plasma membrane from control mice (*n* = 14 recordings from 4 mice) (A). Defective $K_{ATP}$ channel closure in β-cells from PKm1-KO (*n* = 20 recordings from 5 mice) (B) is rescued by PKa pretreatment (*n* = 6 recordings from 3 mice) (C) and acute PKa application (*n* = 7 recordings from 3 mice) (D). PKm1 is sufficient for $K_{ATP}$ closure in β-cells from PKm2-βKO (*n* = 6 recordings from 3 mice) (E). ATP, 1 mM; ADP, 0.5 mM ADP + 0.1 mM ATP; PEP, 5 mM; PKa, 10 µM TEPP-46.

Data are shown as mean ± SEM. *$P < 0.05$, **$P < 0.01$, ***$P < 0.001$, **** $P < 0.0001$ by paired t-test. $^{(*)}P < 0.05$ by unpaired t-test in (H).

# Figure 3

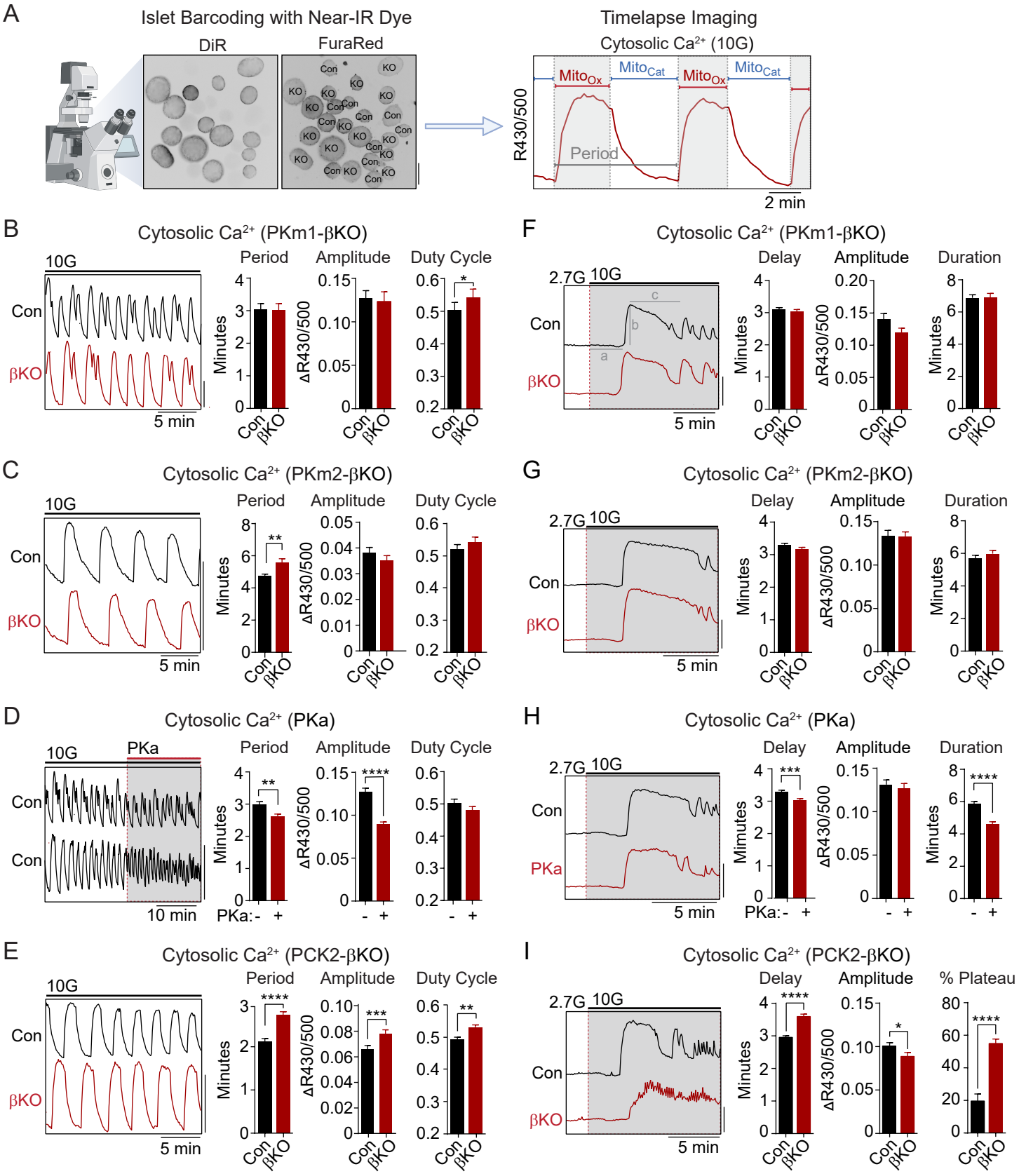
A
Islet Barcoding with Near-IR Dye
DiR
FuraRed
Timelapse Imaging
Cytosolic Ca2+ (10G)
MitoOx
MitoCat
MitoOx
MitoCat
R430/500
Period
2 min
B
Cytosolic Ca2+ (PKm1-βKO)
10G
Con
βKO
5 min
Period
Amplitude
Duty Cycle
Minutes
ΔR430/500
C
Cytosolic Ca2+ (PKm2-βKO)
D
Cytosolic Ca2+ (PKa)
PKa
10 min
PKa:- +
E
Cytosolic Ca2+ (PCK2-βKO)
F
Cytosolic Ca2+ (PKm1-βKO)
2.7G
Delay
Duration
G
Cytosolic Ca2+ (PKm2-βKO)
H
Cytosolic Ca2+ (PKa)
Mimutes
I
Cytosolic Ca2+ (PCK2-βKO)
% Plateau

**Figure 3. PKm2 and PCK2, but not PKm1, have metabolic control over first-phase and steady-state $Ca^{2+}$ influx in response to glucose.**

(A) Barcoding of islet preparations with near-IR dye (DiR) permits simultaneous timelapse imaging of islet $Ca^{2+}$ dynamics of control and βKO mice (scale bar = 200 μm) (*left*). A representative trace illustrates the cataplerotic triggering phase ($Mito_{Cat}$) and oxidative secretory phases ($Mito_{Ox}$) of steady-state $Ca^{2+}$ oscillations in the presence of 10 mM glucose and 1 mM leucine (*right*). Gray line denotes the period.

(B-E) Representative traces and quantification of period, amplitude, and duty cycle of steady-state $Ca^{2+}$ oscillations in islets from PKm1-βKO (*n* = 91 islets from 3 mice) and littermate controls (*n* = 94 islets from 3 mice) (B), PKm2-βKO (*n* = 118 islets from 4 mice) and littermate controls (*n* = 111 islets from 4 mice) (C), control mice treated with PKa (10 μM TEPP-46) (*n* = 88 islets from 3 mice), and PCK2-βKO (*n* = 74 islets from (10G) and 1 mM leucine. Scale bars: 0.1 FuraRed excitation ratio (R430/500).

(F-I) Representative $Ca^{2+}$ traces and quantification of time to depolarization (a), first-phase amplitude (b), and first-phase duration (c) in islets from PKm1-βKO (*n* = 144 islets from 6 mice) and littermate controls (*n* = 150 islets from 6 mice) (B), PKm2-βKO (*n* = 52 islets from 2 mice) and littermate controls (*n* = 55 islets from 2 mice) (C), PKa-treated (10 μM TEPP-46) (*n* = 161 islets from 9 mice) and vehicle controls (*n* = 212 islets from 9 mice) (D), and PCK2-βKO (*n* = 73 islets from 3 mice) and littermate controls (*n* = 78 islets from 3 mice) (E). The bath solution (PSS) contained 1 mM leucine and 2.7 mM (2.7G) and 10 mM glucose (10G) as indicated. Scale bars: 0.1 FuraRed excitation ratio (R430/500).

Data are shown as mean ± SEM. *$P < 0.05$, **$P < 0.01$, ***$P < 0.001$, **** $P < 0.0001$ by unpaired t-test (A-C and E-I) and paired t-test (D).

# Figure 4

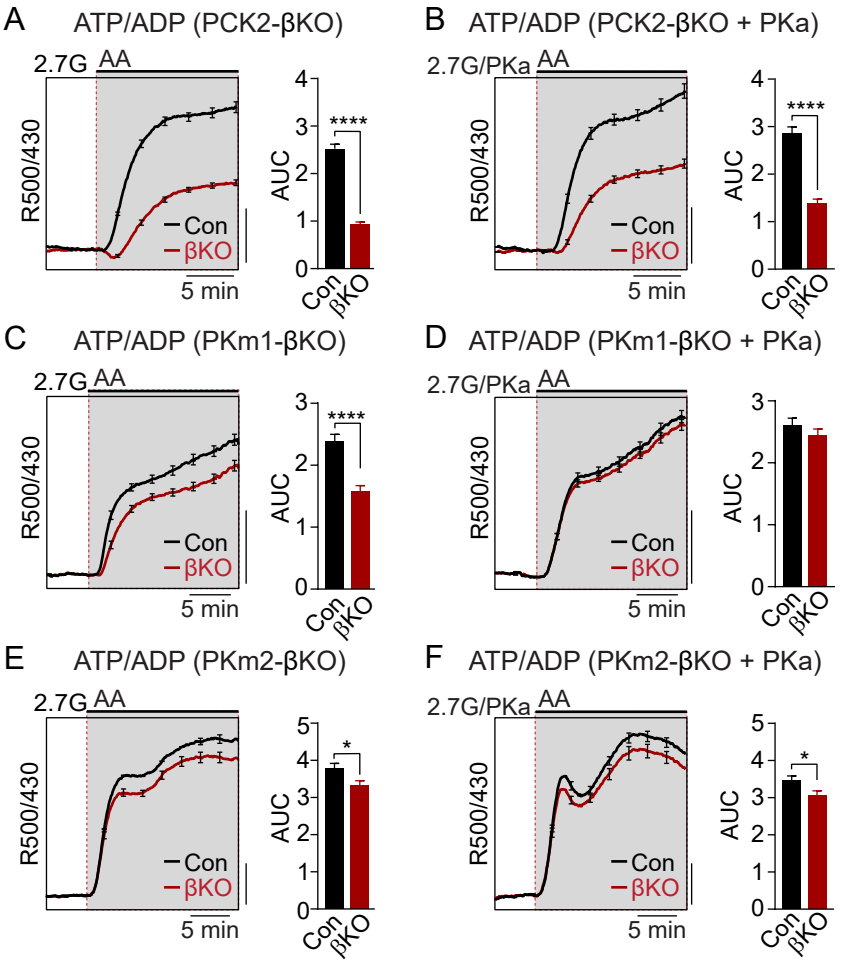
A
ATP/ADP (PCK2-βKO)
2.7G
AA
R500/430
Con
βKO
5 min
AUC
****
Con
βKO
B
ATP/ADP (PCK2-βKO + PKa)
2.7G/PKa
AA
R500/430
Con
βKO
5 min
AUC
****
Con
βKO
C
ATP/ADP (PKm1-βKO)
2.7G
AA
R500/430
Con
βKO
5 min
AUC
****
Con
βKO
D
ATP/ADP (PKm1-βKO + PKa)
2.7G/PKa
AA
R500/430
Con
βKO
5 min
AUC
Con
βKO
E
ATP/ADP (PKm2-βKO)
2.7G
AA
R500/430
Con
βKO
5 min
AUC
*
Con
βKO
F
ATP/ADP (PKm2-βKO + PKa)
2.7G/PKa
AA
R500/430
Con
βKO
5 min
AUC
*
Con
βKO

**Figure 4. Restriction of the glycolytic PEP supply reveals the importance of PCK2 for cytosolic ATP/ADP.**

Average β-cell ATP/ADP in islets from PCK2-βKO (A-B), PKm1-βKO (C-D), and PKm2-βKO (E-F) mice in response to mixed amino acids (AA) provided at three times their physiological concentrations (1x = Q, 0.6 mM; L, 0.5 mM; R, 0.2 mM; A, 2.1 mM) in the presence of 2.7 mM glucose (2.7G) to remove the enolase contribution to cytosolic PEP. PKa (10 μM TEPP-46) was present in B, D, and F. ATP/ADP is quantified as area under the curve (AUC) from PCK2-βKO (vehicle, $n$ = 73 islets from 3 mice; PKa, $n$ = 71 islets from 3 mice) and littermate controls (vehicle, $n$ = 90 islets from 3 mice; PKa, $n$ = 77 islets from 3 mice); PKm1-βKO (vehicle, $n$ = 66 islets from 3 mice; PKa, $n$ = 72 islets from 3 mice) and littermate controls (vehicle, $n$ = 69 islets from 6 mice; PKa, $n$ = 69 islets from 3 mice); and PKm2-βKO (vehicle, $n$ = 99 islets from 3 mice; PKa, $n$ = 89 islets from 3 mice) and littermate controls (vehicle, $n$ = 100 islets from 6 mice; PKa, $n$ = 85 islets from 3 mice). Scale bars: 0.1 Perceval-HR excitation ratio (R500/430).

Data are shown as mean ± SEM. *$P < 0.05$, **** $P < 0.0001$ by t-test.

# Figure 5

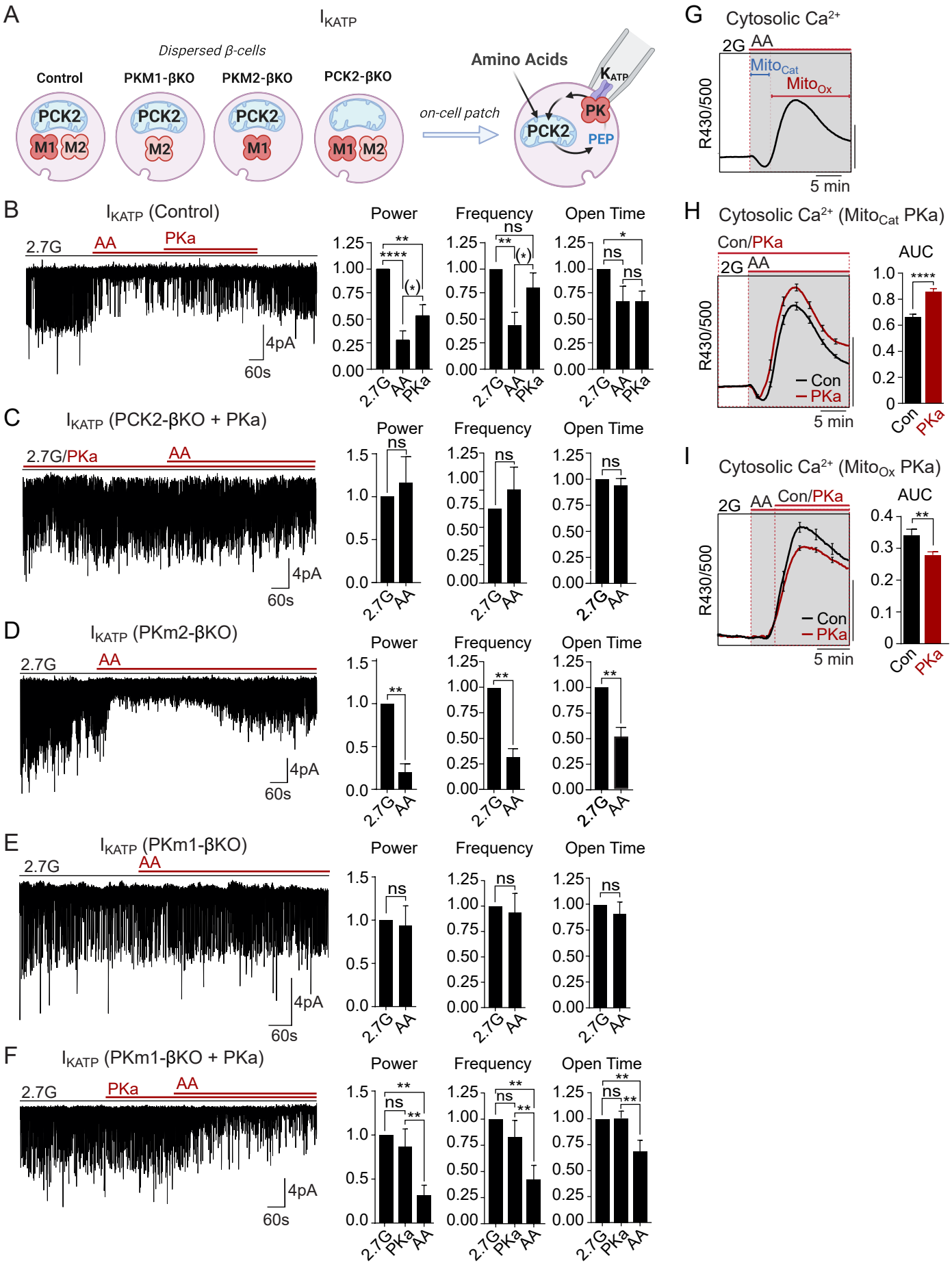
A
$I_{KATP}$
Dispersed β-cells
Control
PKM1-βKO
PKM2-βKO
PCK2-βKO
PCK2
M1
M2
on-cell patch
Amino Acids
$K_{ATP}$
PK
PEP
B
$I_{KATP}$ (Control)
2.7G
AA
PKa
4pA
60s
Power
Frequency
Open Time
C
$I_{KATP}$ (PCK2-βKO + PKa)
2.7G/PKa
D
$I_{KATP}$ (PKm2-βKO)
E
$I_{KATP}$ (PKm1-βKO)
F
$I_{KATP}$ (PKm1-βKO + PKa)
G
Cytosolic $Ca^{2+}$
$Mito_{Cat}$
$Mito_{Ox}$
R430/500
5 min
H
Cytosolic $Ca^{2+}$ ($Mito_{Cat}$ PKa)
Con/PKa
AUC
Con
PKa
I
Cytosolic $Ca^{2+}$ ($Mito_{Ox}$ PKa)

**Figure 5. Mitochondrial PEP signals to PK within the plasma membrane $K_{ATP}$ channel microcompartment in intact β-cells.**

(A) Diagram of on-cell patch clamp method in intact β-cells with bath application of amino acids.

(B-F) Representative example traces and quantification of $K_{ATP}$ channel closure in terms of normalized power, frequency, and open time for β-cells from control (*n* = 10 recordings from 3 mice) (B), PCK2-βKO mice (*n* = 10 recordings from 3 mice) (C), PKm2-βKO (*n* = 7 recordings from 3 mice) (D), PKm1-βKO (*n* = 7 recordings from 3 mice) (E-F) in response to mixed amino acids (AA) and 2.7 glucose (2.7G) as in Figure 4.

(G-I) AA-stimulated $Ca^{2+}$ responses in control islets illustrating the $Mito_{Cat}$ and $Mito_{Ox}$ phases (A). The average $Ca^{2+}$ response to PKa application during $Mito_{Cat}$ (vehicle, *n* =101 islets from 3 mice; PKa, *n* = 99 islets from 3 mice) (H) and $Mito_{Ox}$ (vehicle, *n* = 91 islets from 4 mice; PKa, *n* = 108 islets from 4 mice) (I) is quantified as AUC. Scale bars: 0.025 FuraRed excitation ratio (R430/500).

Data are shown as mean ± SEM. *$P < 0.05$, **$P < 0.01$, ***$P < 0.001$, **** $P < 0.0001$ by paired one-way ANOVA or paired t-test as appropriate. Following the removal of one outlier by ROUT (Q=10%), $^{(*)}P < 0.05$ by paired t-test in (B).

# Figure 6

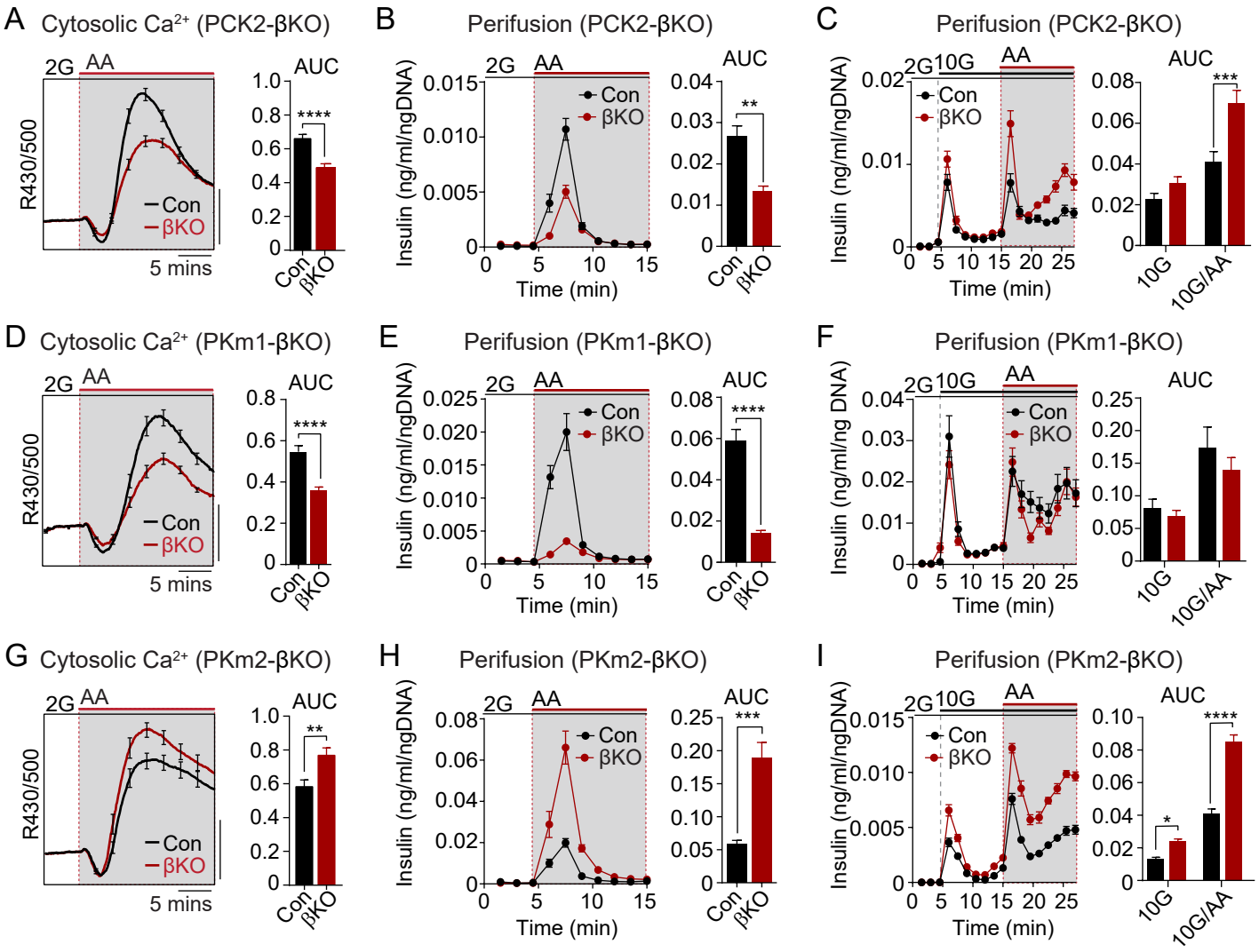
A
Cytosolic Ca2+ (PCK2-βKO)
2G
AA
R430/500
Con
βKO
5 mins
AUC
****
Con
βKO
B
Perifusion (PCK2-βKO)
2G
AA
Insulin (ng/ml/ngDNA)
Con
βKO
Time (min)
AUC
**
Con
βKO
C
Perifusion (PCK2-βKO)
2G
10G
AA
Insulin (ng/ml/ngDNA)
Con
βKO
Time (min)
AUC
***
10G
10G/AA
D
Cytosolic Ca2+ (PKm1-βKO)
2G
AA
R430/500
Con
βKO
5 mins
AUC
****
Con
βKO
E
Perifusion (PKm1-βKO)
2G
AA
Insulin (ng/ml/ngDNA)
Con
βKO
Time (min)
AUC
****
Con
βKO
F
Perifusion (PKm1-βKO)
2G
10G
AA
Insulin (ng/ml/ng DNA)
Con
βKO
Time (min)
AUC
10G
10G/AA
G
Cytosolic Ca2+ (PKm2-βKO)
2G
AA
R430/500
Con
βKO
5 mins
AUC
**
Con
βKO
H
Perifusion (PKm2-βKO)
2G
AA
Insulin (ng/ml/ngDNA)
Con
βKO
Time (min)
AUC
***
Con
βKO
I
Perifusion (PKm2-βKO)
2G
10G
AA
Insulin (ng/ml/ngDNA)
Con
βKO
Time (min)
AUC
*
****
10G
10G/AA

**Figure 6. The PKm1/PKm2 ratio dictates the β-cell $Ca^{2+}$ and secretory response to anaplerotic fuels.**

Average cytosolic $Ca^{2+}$ and insulin secretory responses in controls and PCK2-βKO (A-C), PKm1-βKO (D-F) and PKm2-βKO islets (G-I) to the indicated concentrations of glucose (2G, 2 mM; 10G, 10 mM) and amino acids (AA; concentrations are listed in Figure 4). Data are quantified as AUC. Islet $Ca^{2+}$ data reflect $n$ = 60-101 islets from 3 mice per condition (scale bar = 0.025 FuraRed excitation ratio). Islet perifusion data reflect $n$ = 100 islets per mouse and 6 mice per condition except PKm2-βKO at high glucose (5 mice).

Data are shown as mean ± SEM. *p<0.05, **p<0.01, ***p<0.001, ****p<0.0001 by t-test.